NANO LETTERS

pubs.acs.org/NanoLett

Broadband Light Absorption Enhancement in Thin-Film Silicon Solar Cells

Wei Wang,[†] Shaomin Wu,[†] Kitt Reinhardt,[‡] Yalin Lu,*[,§] and Shaochen Chen*[,∥]

[†]Materials Science and Engineering and [∥]Mechanical Engineering Department, The University of Texas at Austin, Austin, Texas 78712, [‡]United States Air Force Office of Scientific Research, AFOSR/NE, 875 North Randolph Street, Suite 326, Arlington, Virginia 22203, and [§]Laser Optics Research Center, Physics Department, United States Air Force Academy, Colorado 80840

ABSTRACT Currently, the performances of thin film solar cells are limited by poor light absorption and carrier collection. In this research, large, broadband, and polarization-insensitive light absorption enhancement was realized via integrating with unique metallic nanogratings. Through simulation, three possible mechanisms were identified to be responsible for such an enormous enhancement. A test for totaling the absorption over the solar spectrum shows an up to ~30% broadband absorption enhancement when comparing to bare thin film cells.

KEYWORDS Thin film solar cells, broadband absorption enhancement, surface plasmon polaritons, nanogratings, polarization-insensitive.

Active materials used in thin film solar cells are usually polycrystalline or amorphous silicon (*p*-Si or *a*-Si) because of their low cost, nontoxicity, abundance, and mature processing technology. Yet, such great benefits are balanced by a short carrier diffusion length in silicon, resulting in a much lower conversion than that in crystalline solar cells. To achieve a nearly complete absorption the absorbing layer's thickness should be at least a few micrometers. Unfortunately, this is unrealistic because of high and defect-related carrier recombination.[1] As a result, improving the absorption in thin film Si solar cells has become crucial. In the past years, many light-trapping techniques have been investigated, among which a typical example is the use of scattering surface textures.[2] However, they are balanced by the induced surface roughness that is almost of the same order as the film thickness and by the resulting large surface area which causes an increased surface recombination. Recently, notable progresses in the field of surface plasmon polaritons (SPPs)[3] have provided a promising way of light-trapping and have consistently drawn an increasing amount of attention.[4−9]

Upon excitation, SPPs cause strong near-field amplitude of the incident electromagnetic (EM) field, and a resonantly enhanced scattering cross section (SCS) as well. With regard to light absorption enhancement in thin film solar cells, SPPs are thought to be useful because the dissipation energy is proportional to the electric field (E-field) squared, a larger E-field causes a larger absorption, and because a stronger SCS redirects more incident photons into the absorbing layer, substantially increasing the absorbing length. Early work in this area carried out in late 1990s involved incorporation of small copper or silver clusters in organic solar cells, reporting an increase in short circuit current by a factor of 2.[10,11] More recently, Au or Ag nanoparticles[7,9] and nanogratings[5] have been introduced to crystalline[7,9] and amorphous[5,12] silicon solar cells. Common disadvantages associated with those past efforts are that resonances can only occur at certain wavelengths, and their designs involve the use of metallic nanostructures directly on top of solar cells, which will block a fairly large amount of total incident solar photons.[5,6,8] Even more unfortunate, excitation of SPPs is normally very polarization-sensitive to incident radiation. Placing a single scattering object on back side of the cell shows the potential to enhance the absorption;[13] however, using such a simple design to maximize the performance over either a broad spectrum or a large scale will be still a challenge.

In this research, a new thin film solar cell design, placing a metallic nanograting at the bottom of the optically active layer, was proposed. This design will not only free up those photons blocked by surface nanostructures in previous designs, but also achieve a broadband and polarization-insensitive absorption enhancement by taking advantage of effective coupling to planar waveguide modes, the Fabry−Perot (FP) resonance and the SPPs resonance. The design was carefully examined by the two-dimensional (2D) finite element method, and contribution from all above three mechanisms was carefully analyzed. A remarkable ~30% light absorption improvement was anticipated from using the design, when compared to those bare *a*-Si thin film solar cells, and ~10% in certain wavelength ranges, when compared to bulk Si solar cells. Fabrication of such metallic nanogartings is technically feasible too. It can be made by a

* To whom correspondence should be addressed. E-mail: (S.C.) scchen@mail.utexas.edu; (Y.L) yalin.lu@usafa.edu.

Received for review: 12/7/2009
Published on Web: 05/06/2010

DOI: 10.1021/nl904057p | *Nano Lett.* **2010,** *10,* 2012–2018

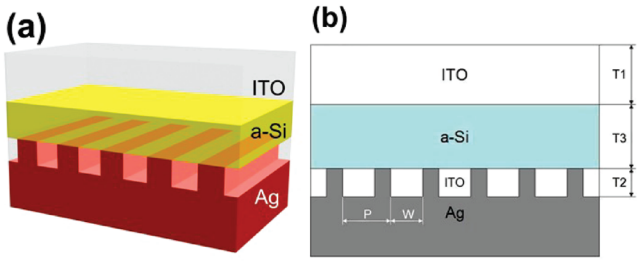

FIGURE 1. The proposed solar cell structure. (a) A 3D conceptual schematic. (b) A cross-sectional view outlining the device's structure to be used in simulations.

few advanced nanofabrication methods[14,15] or simply by aligning the surface with metallic nanowires.[16]

The basic structure of the proposed design is shown in Figure 1. On top is a thin layer of indium tin oxide (ITO) having a thickness of T_1, acting as the top transparent electrode. The bottom electrode is a metallic nanograting with a feature period of P, thickness of T_2, and width of W. The grating slits can be filled with suitable dielectric materials, providing an additional ability to fine-tune the dielectric environment of the nanograting. The light-absorbing Si thin film is then sandwiched between two electrodes, with a thickness of T_3. Solar light will irradiate the cell from the top with TE and TM polarizations. To maximize the absorption, it is important to study the absorption's dependence on the structure's geometric parameters and incident polarizations. To simplify our discussions, we fixed the ITO's thickness, T_1, at 20 nm and the slit width, W, at 100 nm.

To match the solar spectrum to *a*-Si absorption, a wavelength range from 270 to 970 nm was selected. The simulated solar cell structure includes the use of ITO as top electrode, *a*-Si as absorbing material and Ag as bottom electrode, respectively. Dispersive dielectric constants of the three materials can be referred from refs 17−19. The grating slits will be filled with either ITO or spin-on-glass (SOG). In our simulations, EM field distribution across the structure and light absorption by the active *a*-Si layer were analyzed. EM fields were assumed to be time harmonic and the resulting governing equations for the steady-state distribution were solved using a commercial 2D finite element software (COMSOL 3.3).[20] The computational domain considered is a single unit cell surrounded either by periodic boundary conditions or by perfectly matching layers.[21] The absorption by the *a*-Si layer for a normal incident monochrome plane wave was calculated using eq 1

$$\text{Absorption} = \oint_s \vec{S}(\vec{r}, \omega) \cdot d\vec{a} \qquad (1)$$

where $\vec{S}(\vec{r},\omega)$ is the Poynting vector and s is the surface of the analyzed Si layer.

Figure 2a,b shows the simulated E-field distribution across the bare *a*-Si thin film solar cell without the bottom

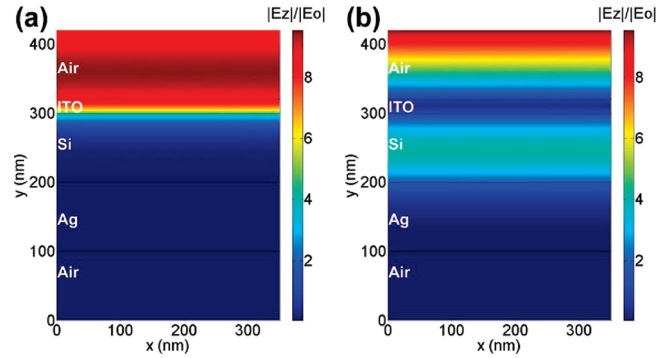

FIGURE 2. Normalized and time-averaged E-field intensity distribution across the basic a-Si solar cell structure at the case of normal incidence. The wavelengths are 270 nm (UV) (a) and 960 nm (near-infrared) (b), respectively. The cell uses a 100 nm thick a-Si layer.

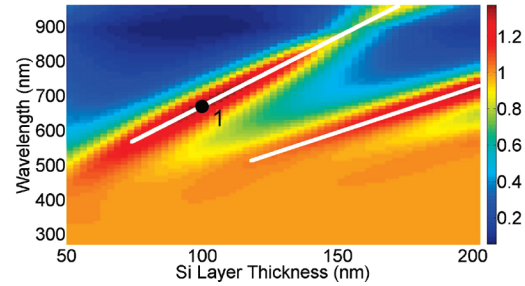

FIGURE 3. Plot of light absorption ratio in a basic cell using a 100 nm thick thin film a-Si to that using a semi-infinite Si layer. The incidence was assumed to be at normal.

Ag nanograting. Under the illumination of an ultraviolet (UV) wavelength of 270 nm (Figure 2a), the incoming photon energy was fully absorbed before reaching the bottom electrode. In the case of illuminating by a near-infrared wavelength light of 960 nm, light reached the bottom electrode and was then reflected back with only a limited amount of photons being absorbed by the *a*-Si layer. A more informative way to see this is to plot the ratio of light absorption in the basic cell using a bare 100 nm thick *a*-Si thin film to that using a semi-infinite Si layer (see Figure 3). Figure 3 shows that for short wavelengths the ratios are close to unity, indicating that the absorption by thin film *a*-Si is comparable to that by the bulk Si. However, for long wavelengths the ratio falls below unity, to a minimum <20 % at certain wavelengths.

Interestingly, in the long wavelength range Figure 3 shows a few areas in which large light absorption enhancement occurs (marked with two white solid lines). This is due to the cavity resonance inside the *a*-Si layer, when both layer thicknesses and the incidence wavelength satisfy the resonance condition. Absorption is then enhanced by the much-intensified E-field inside the *a*-Si layer. Apparently, the wavelength band corresponding to such an enhancement is narrow. Adding an Ag nanograting into the basic cell structure may significantly improve the absorption. To make the comparison straightforward, an absorption enhance-

DOI: 10.1021/nl904057p | *Nano Lett.* **2010,** *10,* 2012--2018

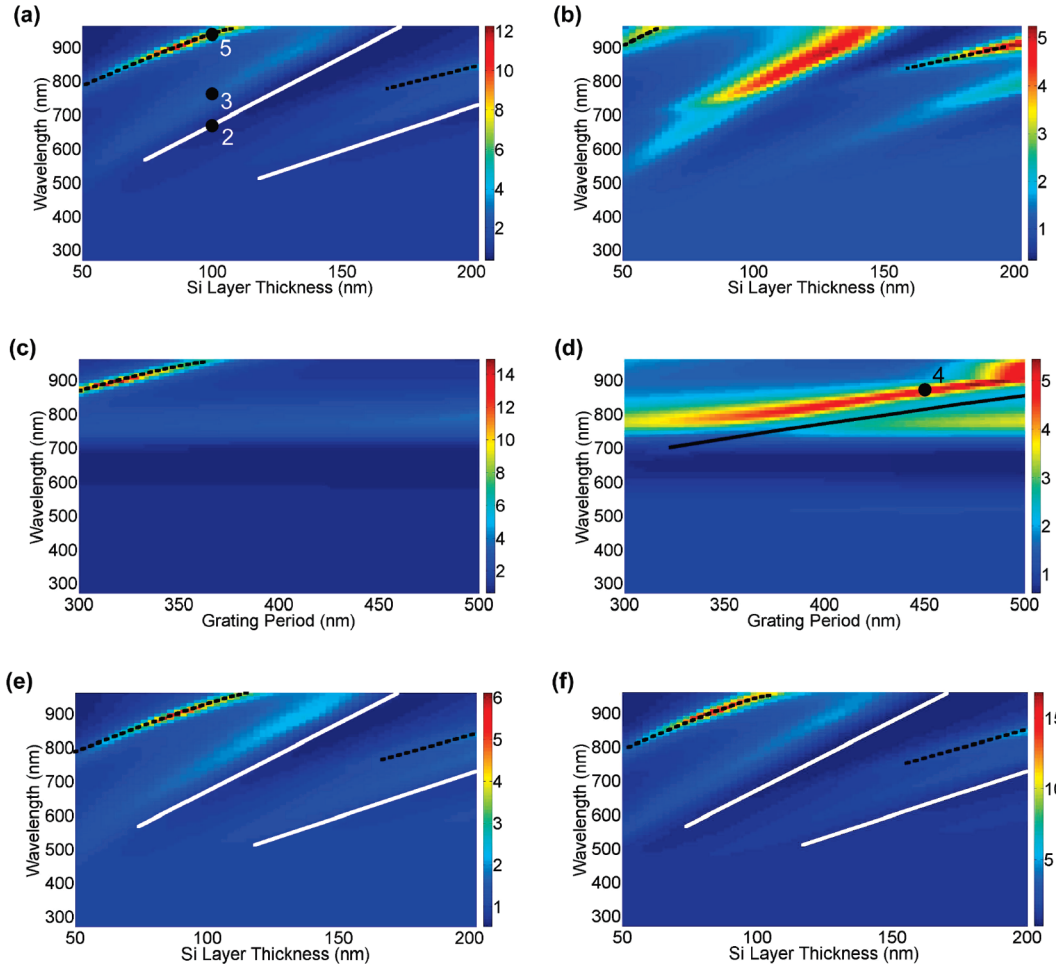

FIGURE 4. Mapping the absorption enhancement with varying geometric parameters and illumination conditions. For all nanograting-added cases, the grating slits were filled with ITO. (a,b) Absorption enhancement with both wavelength and *a*-Si thickness for TE and TM incidences, respectively. The nanograting's periodicity and thickness are 350 and 50 nm, respectively. (c,d) Enhancement versus both wavelength and nanograting's period. The *a*-Si layer thickness was fixed at 100 nm and the nanograting's thickness at 50 nm. Both TE and TM polarizations were considered to account for the randomly polarized nature of sunlight. (e,f) Maps of the absorption enhancement versus both wavelength and film thickness for TE mode only, but the nanograting's thicknesses was changed to 25 nm (e) and 100 nm (f), respectively.

ment function (Λ), defined as the ratio of absorbed energy by the same *a*-Si layer in thin film solar cells with and without adding the Ag nanograting, was used throughout our simulations. Λ is a function of the cell's geometric parameters (nanograting period, *a*-Si layer thickness, slit width, nanograting thickness, etc.), illumination conditions (incidence's wavelength and polarization), and those materials to be used inside the thin film solar cell structure.

Simulation results, obtained through mappings Λ with different structural parameters and incident conditions, are shown in Figure 4a–f. Inside those maps each calculation point represents a full-field simulation result according to corresponding geometric and illumination parameters. For all short wavelengths, adding the Ag nanograting maintains a good absorption, similar to the case without the grating. Significant differences will be (1) the way of absorption enhancement occurring at certain long wavelengths and (2) the broadband absorption enhancement. In Figure 4, the long-wavelength absorption enhancement becomes complicated after adding the nanograting. In some areas (for example in Figure 4c), such an enhancement can reach a level of ~14 times, referring to the intensity bar. A broadband absorption enhancement can also be witnessed in almost every map in Figure 4, and this can be directly attributed to the Ag nanograting. In reality, the ability to realize a large, broadband, and polarization-insensitive absorption enhancement will be crucial to practical thin film solar cells. Results shown here are therefore remarkable.

For a better looking over those figures in Figure 4, both TE and TM wavelength-dependent absorption spectra were shown in Figure 5 (line-cuts when thickness for Si and Ag are fixed at 100 and 50 nm, respectively), selecting the grating period at 350 nm (corresponding to points 2, 3, and 5 in Figure 4a) and 450 nm (the point 4 in Figure 4d), respectively.

In Figure 4, three absorption enhancement mechanisms in the long wavelength range can be identified and are responsible for the observed large, broadband, and polariza-

DOI: 10.1021/nl904057p | *Nano Lett.* **2010,** *10,* 2012–2018

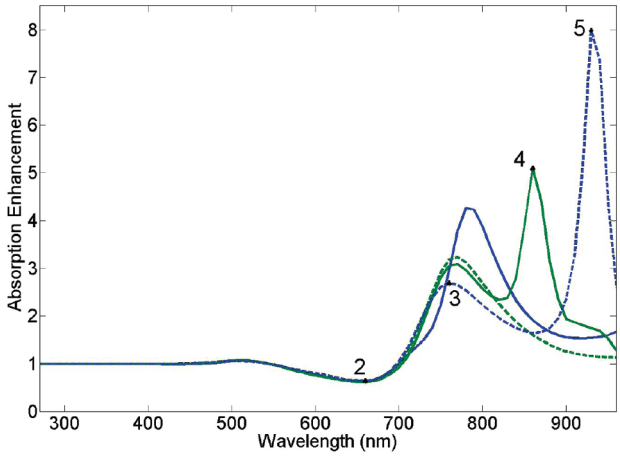

FIGURE 5. Absorption enhancement spectra at the Si thickness of 100 nm, under TM (solid lines) and TE (dashed lines) illumination with the grating periods of 350 nm (blue) and 450 nm (green).

tion-insensitive absorption enhancement. The first mechanism is related to cavity resonance and can be seen in those maps with varying *a*-Si layer thickness, Figure 4a,b,e,f. It is typically dependent on *a*-Si layer thickness and shifts to red when increasing this thickness. The second mechanism directly relates to SPPs, which have characteristics of being excited only by TM polarization, less dependence of plasmonic wavelength on *a*-Si thickness, and red shift as the nanograting's period increases. This can be clearly witnessed through those large enhancements shown in two TM polarization-excited maps, Figure 4b,d. The last mechanism will be associated with coupling into the *a*-Si planar waveguide. Excitation of such planar guiding modes can be affected by *a*-Si layer thickness (Figure 4a,e,f), nanograting period (Figure 4b), and incident polarization (Figure 4b), but much less affected by the nanograting's thickness (Figure 4a,e,f). All such guiding modes are clearly marked in Figure 4a,b,c,e,f with dashed black lines.

In Figure 4a,e,f, the trend of the FP resonance-related enhancement can be referenced by two white solid lines in each map. Such lines are used to mark the FP resonance in the basic cell structure in Figure 3. Clearly, adding an Ag nanograting to the structure causes a large red shift of those FP resonances. To better interpret the FP resonance-related enhancement, Point 1 in Figure 3 was selected as an example. This point represents a combination of wavelength at 670 nm and *a*-Si layer thickness of 100 nm and corresponds to an exact FP resonance in the basic cell structure. After adding a 50 nm thick Ag nanograting with a period of 350 nm, the resonance red shifted to Point 3 in Figure 4a and Figure 5, corresponding to a wavelength at 760 nm, and left a much reduced absorption at the original position of Point 2 (same position as Point 1 in Figure 3). Such results can be further verified by the simulated EM field distributions (Figure 6). Figure 6a,b shows the E-field distributions across the basic cell for wavelengths at 670 nm (Point 1) and 760 nm, respectively. Obviously, the latter is slightly off the FP

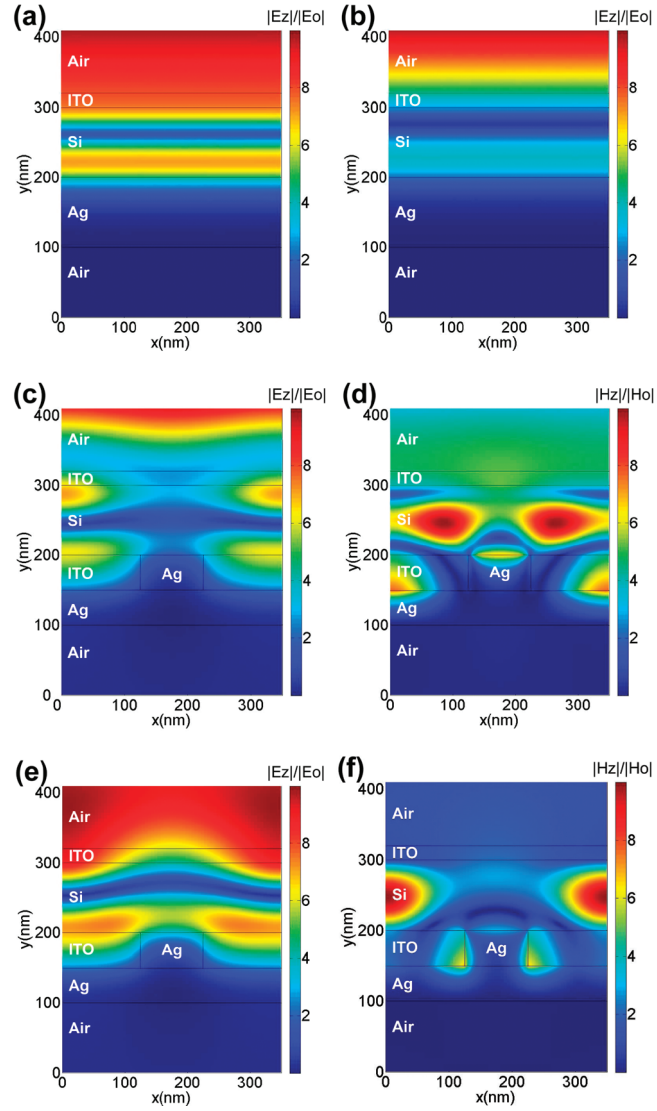

FIGURE 6. Normalized and time-averaged field plots across the cell structure. In all cases, the a-Si layer thickness is 100 nm and the incidence is at normal. (a,b) A bare a-Si layer was illuminated at wavelengths of 670 and 760 nm, respectively. (c,d) The nanograting-added structure illuminated by a wavelength of 670 nm at TE and TM polarizations, respectively. The Ag nanograting has $P = 350$ nm and $T_2 = 50$ nm, and was filled with ITO. (e,f) Similar to (c,d), but the incident wavelength was shifted to 760 nm.

resonance. Figure 6c,e (d,f) shows TE (TM) electric (magnetic) field distributions at Point 2 and 3, respectively. Comparing to Figure 6c, Figure 6e shows a much enhanced electric field intensity inside the *a*-Si layer at the wavelength of 760 nm, indicating a red shift after adding the Ag nanograting. It is reasonable to assume that adding an Ag nanograting will actually change the effective cavity thickness, which causes the red shift. According to Figure 4a,e,f, the red shift can also be affected by the Ag nanograting's thickness. Therefore, adjusting the Ag nanograting will be a practical means to tune the FP resonance (under both TE and TM polarizations) to better fit the solar spectrum without the need to change the *a*-Si layer thickness.

DOI: 10.1021/nl904057p | *Nano Lett.* **2010,** *10,* 2012--2018

Presence of an Ag nanograting increases the usefulness of TM polarization, according to the results shown in Figure 4b,d in which as high as 5 times enhancement can be expected. To verify the judgment that such an enhancement is from TM polarization-excited SPPs, the relationship between the SPP wavelength and nanograting period was analyzed, and compared to the observed enhancement features shown in Figure 4d. At the interface between two materials with dielectric constant ε_1 and ε_2, the SPP wavevector will be given by[22]

$$\mathbf{k}_{sp} = \mathbf{k}_0\left(\frac{\varepsilon_1\varepsilon_2}{\varepsilon_1 + \varepsilon_2}\right)^{1/2} \quad (2)$$

here $\mathbf{k}_{sp}$ is parallel to the interface and k_0 is wavevector at vacuum. Since ε_1 and ε_2 are opposite in sign (at least one material is conductive), $\mathbf{k}_{sp}$ is greater than the maximum photon wavevector available in the dielectric. The mismatch in wavevector between the in-plane momentums can be achieved by patterning the metal with a shallow grating of grooves having a period P. For a simple and one-dimensional (1D) grating, phase matching will take place at[22]

$$\mathbf{k}_{sp} = \mathbf{k}_x \pm 2n\pi/P \quad (3)$$

At the normal incidence, $\mathbf{k}_x$ goes to zero. With $n = 1$, substituting eq 3 into eq 2 results in eq 4, the requirement to excite SPPs with the metallic 1D grating

$$2\pi/P = \mathbf{k}_0\left(\frac{\varepsilon_1\varepsilon_2}{\varepsilon_1 + \varepsilon_2}\right)^{1/2} \quad (4)$$

Here the interface is between ITO and silver ($\varepsilon_1 = \varepsilon_{ITO}$ and $\varepsilon_2 = \varepsilon_{Ag}$). Since ε_{ITO}, ε_{Ag}, and $\mathbf{k}_0$ are functions of free space wavelengths, the SPP wavelength can be simplified as a function of the grating period. The estimated result is shown in Figure 4d as a black solid line. The trend of this line matches well with the observed absorption enhancement features, and this supports the previous SPP-related absorption enhancement argument. A clear offset between the line and the observed absorption feature is due to the used approximation. In fact, ε_1 should be a complicated function of grating period, grating slit size, dielectric constants of ITO and Si, and so forth.

To look at the process more closely, Point 4 in Figure 4d, corresponding to a wavelength of 860 nm and a grating period of 450 nm, was carefully analyzed. The simulated EM field distribution across the cell with an Ag nanograting (Figure 7b) shows a much stronger H_z field inside the a-Si layer, when compared to the case without the Ag nanograting (Figure 7a). The argument that this enhancement is produced by SPPs can be supported by the strong H_z field observation around both Si/Ag and ITO/Ag interfaces (also found in Figure 6d and 6f). This behavior indicates an existence of plasmonic current-a clear indication of TM polarization excited SPPs.

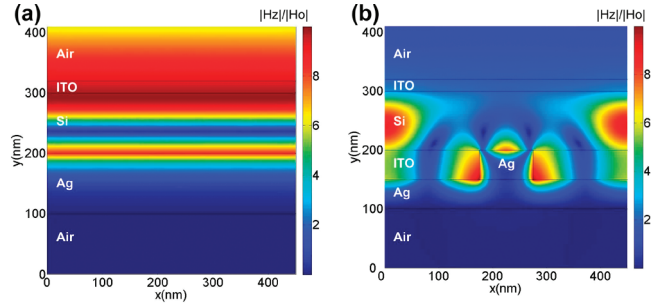

FIGURE 7. Normalized and time-averaged field plots across the cell structure. (a) A bare a-Si layer was illuminated at wavelength 860 nm. (b) An Ag nanograting with $P = 450$ nm, $T_2 = 50$ nm was added, and the grating was filled with ITO. The incoming light is a TM-polarized beam having a wavelength at 860 nm also.

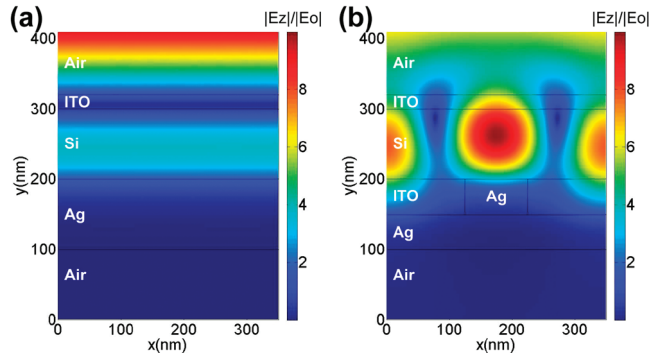

FIGURE 8. Normalized and time-averaged field plots across the cell structure. (a) A bare Si layer was illuminated at wavelength 930 nm. (b) A metallic grating structure was added with $P = 350$ nm, $T_2 = 50$ nm (Figure 1), and the grating slits were filled with ITO. The incoming light is TE polarized with the same wavelength as (a).

A major contribution to the observed absorption enhancement is from lateral coupling of incident photons. In our designs, enhancement features from the lateral coupling can be found in Figure 4a–c,e,f, all marked with dashed black lines. The simulated E-field distributions corresponding to Point 5 in Figure 4a show a strong field pattern similar to that in ref 6 (Figure 8a). The guiding mode weakens when removing the Ag nanograting (Figure 8b). Formation of such strong field patterns is due to the excitation of guiding modes in the planar a-Si slab waveguide.[23] Very strong enhancement (up to 14 times) can occur in the near-infrared regime for both TE and TM illuminations after adding the Ag nanograting. This enhancement red shifts with a thicker Si layer, a larger grating period and a thicker Ag nanograting.

To perform a full evaluation on the design, total absorption enhancement over the full solar spectrum must be considered. Normally, a solar cell's short circuit current is proportional to the number of photons being absorbed.

DOI: 10.1021/nl904057p | *Nano Lett.* **2010,** *10,* 2012–2018

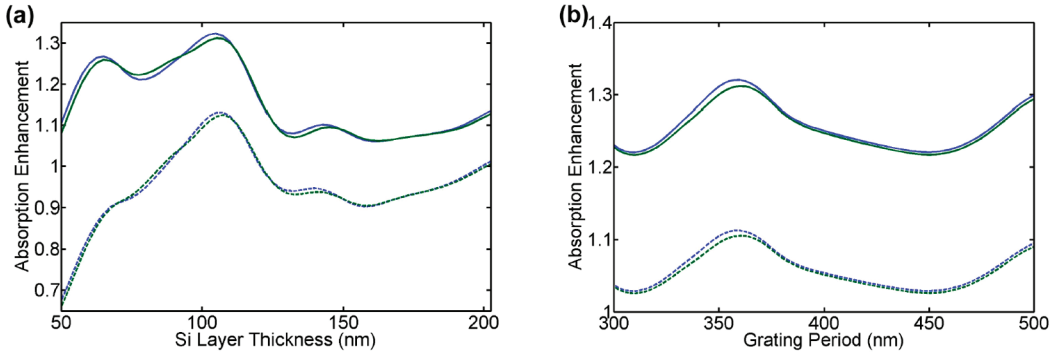

FIGURE 9. Total absorption enhancement over the full solar spectrum. (a) Absorption enhancement compared with bare thin layer *a*-Si (solid lines) and semi-infinite (bulk) Si layer (dashed lines) as a function of *a*-Si thickness with grating period at 350 nm. (b) Absorption enhancement as a function of grating periodicity with a-Si layer thickness at 100 nm (solid lines) and semi-infinite Si layer (dashed lines). The grating slits were filled with ITO (blue) and SOG (green).

Therefore, total absorption enhancement must be evaluated based on the absorbed photon number. Assuming that distribution of the normalized photon number is a function of wavelength, $I(\lambda)$, for the solar emission AM 1.5-G, and considering that the absorption enhancement due to the presence of the Ag nanograting is also a function of illumination (therefore, $\Lambda_{TM}(\lambda)$ and $\Lambda_{TE}(\lambda)$ were assumed to be functions representing different incident polarizations), the total absorption enhancement over the entire solar spectrum can be then calculated using

$$\Lambda_{tot} = \frac{1}{2}\left(\int fI(\lambda) \times \Lambda_{TM}(\lambda)d\lambda + \int fI(\lambda) \times \Lambda_{TE}(\lambda)d\lambda\right) \quad (5)$$

where f is a normalized factor, that is, $\int fI(\lambda)d\lambda = 1$.

Two slit filler materials, ITO and SOG, were considered, to see the effect of changing the nanograting's dielectric environment. The dielectric constant of ITO can be found from ref 18. A complete representation for the dielectric constant of SOG will be difficult since that it strongly depends on its curing temperature (ref 19). Therefore it was assumed to have value of $2.7 + 0.01i$. Figure 9a,b shows the enhancement as a function of *a*-Si thickness and Ag nanograting's period, respectively. The nanograting's thickness is 50 nm. The results clearly show that the dielectric environment has little impact on the overall absorption enhancement.

The solid lines in Figure 9a,b, which are the absorption enhancements when compared with a bare *a*-Si thin layer, show that adding the nanograting can enhance the absorption as much as 30%. Furthermore, the enhancement is broadband when varying both *a*-Si layer thickness and the nanograting period. The dashed lines in Figure 9a,b represent the absorption enhancement when compared to bulk Si. It is very remarkable that with the *a*-Si thickness changing from 85 to 120 nm and the grating period from 350 to 370 nm performance of such an Ag nanograting-embedded thin film *a*-Si solar cell can be better than bulk Si-based solar cells. The average enhancement in this range can be above 10%.

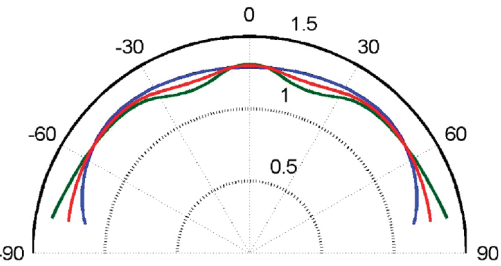

FIGURE 10. Absorption enhancement over the full solar spectrum as a function of the angle of incidence. The absorption was compared to the bare thin layer a-Si under TM (blue), TE (green), and unpolarized (red) illumination, respectively. Both Si thickness and grating period are fixed at 100 and 350 nm, respectively. The grating slits were filled with SOG.

Finally, we considered the absorption dependency on incident angle, as shown in Figure 10. Total enhancement under an unpolarized illumination with an incident angle from 0−82 °C is floating between 24 and 31%, indicating that the response is relatively immune to the incident angle.

In conclusion, a unique thin film Si solar cell design which includes an embedded metallic nanograting was proposed. While maintaining a similar absorption in the short wavelength range, large, broadband, and polarization-insensitive absorption enhancement can be realized in the long wavelength range (visible to infrared) when adding a thin metallic nanograting. Three mechanisms, the Fabry−Perot resonance, SPPs resonance and planar waveguide coupling, were identified in related to the observed high absorption enhancement. Since this unique solar cell design has no critical geometry requirements, concerns associated with fabrication and cost could be better balanced. Besides the discussed *a*-Si, extending the similar design into other active solar materials such as CdTe and organics can also be expected.

Acknowledgment. Financial support from the U.S. National Science Foundation, the Office of Naval Research and the Air Force Office of Scientific Research (AFOSR) is greatly appreciated. The authors are grateful for the computer support from Intel's Higher Education Program.

DOI: 10.1021/nl904057p | *Nano Lett.* **2010,** *10,* 2012--2018

REFERENCES AND NOTES

(1) Shah, A. V.; Schade, H.; Vanecek, M.; Meier, J.; Vallat-Sauvain, E.; Wyrsch, N.; Kroll, U.; Droz, C.; Bailat, J. Thin-film silicon solar cell technology. *Prog. Photovolt.* **2004**, *12*, 113–142.

(2) Green, M. A. Lambertian light trapping in textured solar cells and light-emitting diodes: analytical solutions. *Prog. Photovolt.* **2002**, *10*, 235–241.

(3) Barnes, W. L.; Dereux, A.; Ebbesen, T. W. Surface plasmon subwavelength optics. *Nature* **2003**, *424*, 824–830.

(4) Hallermann, F.; Rockstuhl, C.; Fahr, S.; Seifert, G.; Wackerow, S.; Graener, H.; von Plessen, G.; Lederer, F. On the use of localized plasmon polaritons in solar cells. *Phys. Status Solidi* **2008**, *205*, 2844–2861.

(5) Rockstuhl, C.; Fahr, S.; Lederer, F. Absorption enhancement in solar cells by localized plasmon polaritons. *J. Appl. Phys.* **2008**, *104*, 123102–7.

(6) Pala, R. A.; White, J.; Barnard, E.; Liu, J.; Brongersma, M. L. Design of Plasmonic Thin-Film Solar Cells with Broadband Absorption Enhancements. *Adv. Mater.* **2009**, *21*, 1–6.

(7) Schaadt, D. M.; Feng, B.; Yu, E. T. Enhanced semiconductor optical absorption via surface plasmon excitation in metal nanoparticles. *Appl. Phys. Lett.* **2005**, *86*, No. 063106−3.

(8) Panoiu, N. C.; Osgood, R. M. Enhanced optical absorption for photovoltaics via excitation of waveguide and plasmon-polariton modes. *Opt. Lett.* **2007**, *32*, 2825–2827.

(9) Pillai, S.; Catchpole, K. R.; Trupke, T.; Green, M. A. Surface plasmon enhanced silicon solar cells. *J. Appl. Phys.* **2007**, *101*, No. 093105−8.

(10) Stenzel, O.; Stendal, A.; Voigtsberger, K.; Vonborczyskowski, C. Enhancement of the photovoltaic conversion efficiency of copper phthalocyanine thin-film devices by incorporation of metal-clusters. *Sol. Energy Mater. Sol. Cells* **1995**, *37*, 337–348.

(11) Westphalen, M.; Kreibig, U.; Rostalski, J.; Luth, H.; Meissner, D. Metal cluster enhanced organic solar cells. *Sol. Energy Mater. Sol. Cells* **2000**, *61*, 97–105.

(12) Derkacs, D.; Lim, S. H.; Matheu, P.; Mar, W.; Yu, E. T. Improved performance of amorphous silicon solar cells via scattering from surface plasmon polaritons in nearby metallic nanoparticles. *Appl. Phys. Lett.* **2006**, *89*, No. 093103−3.

(13) Ferry, V. E.; Sweatlock, L. A.; Pacifici, D.; Atwater, H. A. Plasmonic Nanostructure Design for Efficient Light Coupling into Solar Cells. *Nano Lett.* **2008**, *8*, 4391–4397.

(14) Fan, Z. Y.; Ho, J. C.; Takahashi, T.; Yerushalmi, R.; Takei, K.; Ford, A. C.; Chueh, Y. L.; Javey, A. Toward the Development of Printable Nanowire Electronics and Sensors. *Adv. Mater.* **2009**, *21*, 3730–3743.

(15) Chen, S. *Nanomanufacturing*; American Scientific Publishers: Stevenson Ranch, CA, 2009.

(16) Tao, A. R.; Huang, J. X.; Yang, P. D. Langmuir-Blodgettry of Nanocrystals and Nanowires. *Acc. Chem. Res.* **2008**, *41*, 1662–1673.

(17) Palik, E. D. *Handbook of Optical Constants of Solids*; Academic Press: Orlando, FL, 1985.

(18) Mergel, D.; Qiao, Z. Dielectric modelling of optical spectra of thin In_2O_3: Sn films. *J. Phys. D: Appl. Phys.* **2002**, *35*, 794–801.

(19) Cook, R. F.; Liniger, E. G. Stress-corrosion cracking of low-dielectric-constant spin-on-glass thin films. *J. Electrochem. Soc.* **1999**, *146*, 4439–4448.

(20) *COMSOL 3.3 Reference Manual*; COMSOL AB: Stockholm, 2005.

(21) Lavrinenko, A.; Borel, P. I.; Frandsen, L. H.; Thorhauge, M.; Harpoth, A.; Kristensen, M.; Niemi, T.; Chong, H. M. H. Comprehensive FDTD modelling of photonic crystal waveguide components. *Opt. Express* **2004**, *12*, 234–248.

(22) Maier, S. A. *Plasmonics: Fundamentals and Applications*, 1st ed.; Springer: New York, 2007.

(23) Jackson, J. D. *Classical Electrodynamics*, 3rd ed.; Wiley: New York, 1998.

DOI: 10.1021/nl904057p | *Nano Lett.* **2010,** *10,* 2012--2018